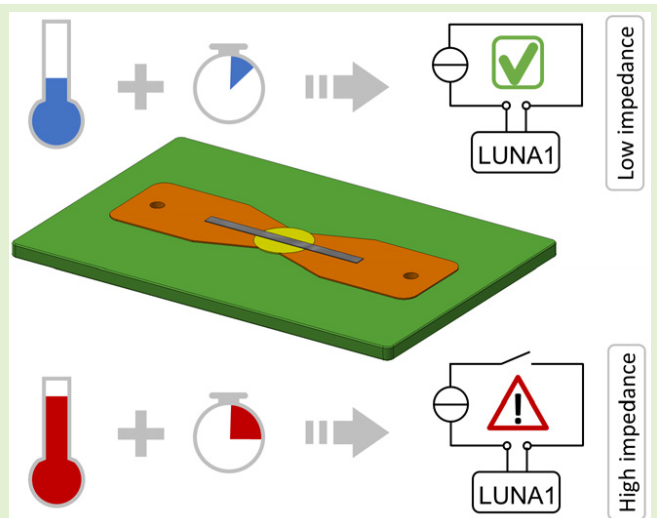


Introducing a Wax-Based Temperature-Time-Dependent Threshold Sensor

René Körbitz¹, Andreas Heinig¹, and Wolf-Joachim Fischer, *Life Senior Member, IEEE*

Abstract—Temperature monitoring is an important tool for a broad variety of sensitive goods to maintain their quality and integrity during supply chain operations. To balance cost and benefit, many applications use sensors that only monitor a specific reference temperature limit. These sensor elements should be lightweight, low cost, and ready for wireless readout. In this work, an innovative sensor concept is presented that can meet these requirements. It irreversibly changes its electrical resistance from low impedance to high impedance if a certain temperature value is violated. The sensor element uses wax as a temperature-dependent element. If its melting temperature is exceeded, the liquid wax starts to flow into a textile reservoir. The descending liquid level of the outflowing wax disrupts an inkjet-printed nanoparticle layer that electrically connects the sensor's input and output contact. A fluidic resistance between wax and textile reservoir regulates the speed of wax flow. Thus, it is possible to set a time delay for triggering the sensor after the threshold temperature is reached. This article demonstrates the feasibility of the proposed sensor concept experimentally. Furthermore, the sensor element is connected to a custom-made radio frequency identification (RFID) tag, which allows wireless readout of the sensor state. From the authors' point of view, the simple functional principle combined with the good scalability of the sensor concept offers a high potential for smart packaging applications.

Index Terms—Ag-nanoparticles, inkjet printing, radio frequency identification (RFID) sensor tag, temperature sensors, threshold value sensor.



I. INTRODUCTION

THE fundamentals of our current economic landscape are global trade and expansive networks of worldwide supply chains. This includes transporting goods over long distances combined with the challenge of maintaining their integrity and quality during all stages of this logistic process. In the food supply chain, around 30% of the produced food is wasted every year due to improper handling and cold chain failures [1], [2]. In addition to the economic damage, there are also ecological and social aspects that should be considered, when talking about supply chain failures. Similar challenges

also arise in other product categories such as electronics, pharmaceutical products, and chemical substances. Also, for these products, certain limits must be adhered to during transportation and storage to ensure quality and integrity. In many cases, temperature is one of the most important parameters, which has to be kept in a certain range. Depending on the product type, this can vary significantly, for instance, from $-25\text{ }^{\circ}\text{C}$ for foods to $50\text{ }^{\circ}\text{C}$ for specific chemical substances, raw materials, or electronic goods [3], [4], [5].

Temperature monitoring is also essential in numerous technical processes and applications in the consumer and healthcare sectors. The sensors used are usually based on thermistors, thermocouples, or temperature-dependent resistors (resistance temperature detectors—RTDs). These sensors can be integrated into networks or used in conjunction with data loggers to enable continuous temperature monitoring [6], [7]. However, such systems are rarely used in supply chains because they require an external power source and are comparatively expensive. Especially in product-level temperature monitoring, the sensor costs play an important role. For this reason, sensors are used in these cases that do not continuously measure the temperature but only detect the exceedance of certain threshold values. Temperature-threshold indicators

Manuscript received 18 August 2023; revised 9 November 2023; accepted 13 November 2023. Date of publication 29 November 2023; date of current version 31 January 2024. This work was supported by the German Federal Ministry of Education and Research (BMBF) through the Project Cool-RFID. The associate editor coordinating the review of this article and approving it for publication was Dr. Anindya Nag. (Corresponding author: René Körbitz.)

René Körbitz and Wolf-Joachim Fischer are with the Chair of Microsystems, Technische Universität Dresden Institut für Halbleiter-technik, 01062 Dresden, Germany (e-mail: rene.koerbitz@tu-dresden.de).

Andreas Heinig is with the Department of Wireless Microsystems, Fraunhofer-Institut für Photonische Mikrosysteme IPMS, 01109 Dresden, Germany.

Digital Object Identifier 10.1109/JSEN.2023.3334792

(TTIs) are usually used for this task. These simple and low-cost labels can be applied directly to the products to be monitored and triggered either after a defined duration of temperature exceedance or when a certain reference temperature is reached [8], [9]. Due to a chemical or biological reaction, they undergo a permanent color change, which can be evaluated visually [10]. However, this requires line-of-sight for reading the sensor information and makes it difficult to integrate the TTIs into digital monitoring systems or networks.

Due to these limitations, the development of simple temperature threshold sensors that do not require continuous power supply and whose state can be evaluated electronically is gaining increasing importance. The outcomes are sensor elements that rely on simple mechanisms, for instance, phase transitions, to detect temperature threshold violations. The sensor's reaction to such an event is usually a significant change in its electrical impedance [11], [12] or frequency response [13], [14], [15]. This enables easy integration of these sensor elements into wireless evaluation systems, for example, based on radio frequency identification (RFID) technology. In this way, the sensor information can be retrieved easily and quickly without requiring direct access to the sensors or packaging.

Many sensors presented in the literature are suitable for monitoring temperature limits but rarely provide an option to define the permitted duration of critical temperature exposure. Bhattacharyya et al. [11] presented a temperature threshold sensor that provides this capability. It is based on detuning the RFID tag signal due to the movement of a metal plate, which is initially fixed by a temperature-sensitive material. The volume of this material sets the triggering delay after exceeding the temperature limit. Although the presented sensor is quite innovative, it has some drawbacks. The temperature-sensitive material affects the RFID signal, which leads to a noticeable decrease in read range. In addition, the design of the sensor allows only vertical application.

In this article, we present the design of a phase transition-based temperature sensor that enables the detection of a user-defined duration of critical temperature load. Furthermore, we demonstrate that the developed sensor element is suitable for integration in passive RFID tags.

II. SENSOR CONCEPT

A. Temperature Threshold Sensor Element

The temperature sensor principle is based on three different mechanisms: 1) temperature threshold detection based on the melting behavior of the wax; 2) time delay setup via a fluidic resistor; and 3) triggering the sensor irreversibly by physical disruption of a printed conductor.

The proposed sensor design is depicted in Fig. 1. The wax, determining the trigger temperature, is stored in a reservoir between two electrical connection pads. Both are linked by a thin conductive layer, which is inkjet printed on the wax surface. Beneath the wax reservoir is an absorbing fabric located, which is separated from the wax by a plate with a thickness of 1 mm and a central hole. As the melting process of the wax proceeds from the outside to the center of the reservoir, the diameter of this hole determines the time at which the

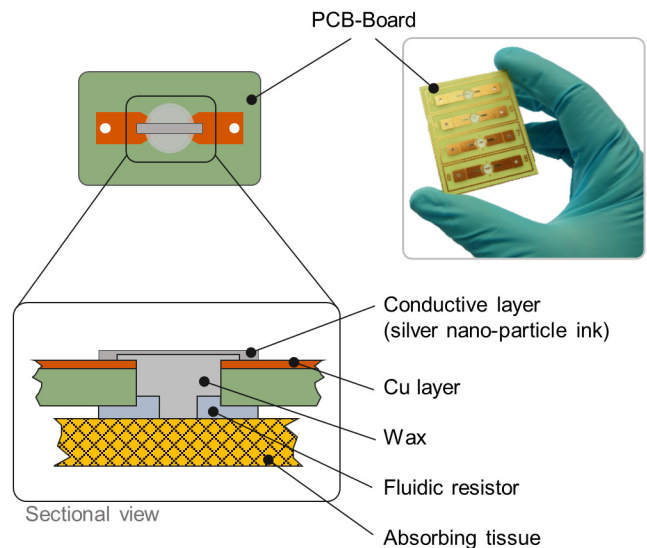


Fig. 1. Schematic representation of the sensor setup.

liquid wax begins to flow into the absorbent tissue. We call this element a fluidic resistor, which basically determines the exposure time for a certain reference temperature.

The sensors' working principle is shown in Fig. 2. Exceeding the sensor elements' target temperature, the wax in the reservoir starts to melt [Fig. 2(b)]. After a specific time, which is defined by the fluidic resistors' geometry, the wax flows into the absorbing tissue and causes a decreasing fluid level in the reservoir. This leads in the end to a cutoff of the conductive layer between the electrical connectors and switches the sensors' impedance from low to high. This irreversible change is the sensor element output to any evaluation circuit [Fig. 2(c)]. To demonstrate the sensor suitability for RFID-based readout, it is connected to an application-specific integrated circuit (ASIC) called LUNA1, which was developed by the Fraunhofer-Institute IPMS, Dresden, Germany [16], [17]. Using the energy provided by the electromagnetic field of an RFID reader, the ASIC can detect, store, and transmit the state of the sensing element. A more detailed description of this process is given in Section II-B.

B. Sensor Transponder LUNA1

The ASIC LUNA1 consists of a programmable microcontroller, 2048 bytes of nonvolatile memory, a state machine for the ISO 18000-6 protocol, and a module for RFID communication and energy harvesting. The microcontroller enables connecting a wide variety of digital sensors, actuators, and analog-to-digital converters to the transponder by serial peripheral interface (SPI), general purpose input/output (GPIO), and inter-integrated circuit (I²C) interfaces. In this work, a pin carrier is used to attach the temperature threshold sensor to the ASIC GPIO port for status monitoring. If the sensor element is triggered, the LUNA1-ASIC detects this change of state as soon as it is supplied with energy from an electromagnetic field of an RFID reader and sets a status bit in its memory area accordingly. Supplementing the ASIC with a planar dipole

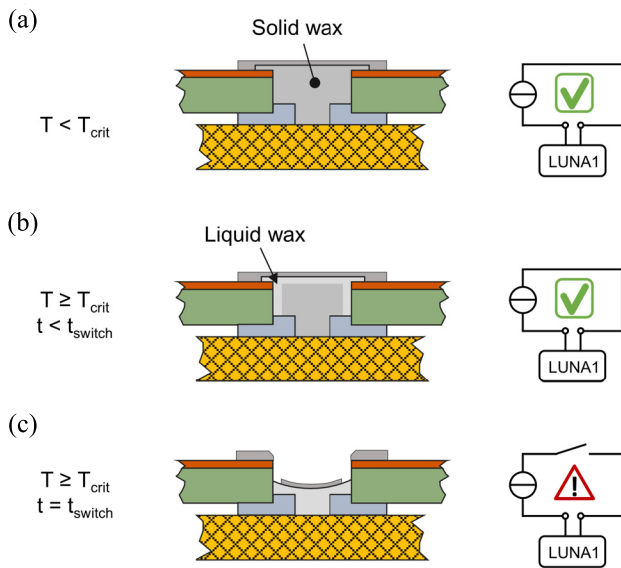


Fig. 2. Working principle of the wax-based temperature threshold sensor: (a) initial state of the sensor element. The temperature is below the critical temperature (T_{crit}) and the electric circuit is closed; (b) temperature exceeds T_{crit} , the wax starts to melt but the fluidic resistor blocks the outflow; and (c) after reaching t_{switch} , the wax flows through the fluidic resistor into the absorbing tissue, which causes an interruption of the electric circuit.

antenna enables the readout of this information via the RFID field by any common ISO 18000-6 reader.

III. MATERIALS AND METHODS

A. Material Characterization

The different waxes were procured from Carl Roth GmbH, Karlsruhe, Germany, H&R Group, Hamburg, Germany, and Deurex AG, Elsteraue, Germany. Melting points of all wax samples were analyzed by differential scanning calorimetry (DSC, TA Instruments, New Castle, DE, USA—MDSC2920). Each sample (8.7–14.2 mg) was filled in an aluminum pan. Thermograms were obtained by scanning from $-10\text{ }^{\circ}\text{C}$ to $160\text{ }^{\circ}\text{C}$ applying a heating rate of 5 K/min . An empty aluminum pan served as a reference. According to the analysis, the measured melting temperatures are in good agreement with the data provided by the manufacturers (Table I).

B. Surface Modification

A characteristic feature of waxes is their low polarity, which leads to an insolubility in water and prevents water-based materials to spread on wax or wax-coated surfaces. Crucial for the temperature sensor elements' working principle is a thin conductive layer fabricated by inkjet printing. As the available silver nanoparticle ink shows a hydrophilic wetting behavior, the wax surface has to be modified to match the ink's wetting properties. Many techniques are available to make wax surfaces less hydrophobic, for example, using bio-products such as enzymes (xylanases), chemicals such as tris (polyoxyethylene) sorbitan monooleate [18], and hydroxymethylated resorcinol (HMR) [19]. Another possible way to improve the wettability of wax surfaces is plasma treatment, which is a relatively simple process and therefore seems to

be the most suitable procedure for the objectives of this work [20], [21].

Surface modification was done by a plasma cleaning device (Diener—Zepto) with an oxygen flow of 20 sccm and an operation power of 20 W. The resulting wetting properties were determined by contact angle measurements (DataPhysics—OCA 20) by applying the sessile drop method. Distilled water was used to form the droplets with a volume of $1\text{ }\mu\text{L}$. The native contact angles were calculated by the averaged data of five droplets. Samples were prepared by coating a microscopy glass slide ($76 \times 26 \times 1\text{ mm}$) with a wax layer of 1 mm thickness. Initial investigations focused on the duration of the plasma treatment. Fig. 3(a) shows this data exemplary for wax 2. It was found that an almost constant contact angle was reached after an exposure time of 90 s, which is in good agreement with [22]. The resulting contact angles for different waxes and their change over time after the modification are shown in Fig. 3(b). The native contact angle is given in brackets behind the wax' name. The data show a considerable change in surface properties after the oxygen plasma treatment. That means in detail, the contact angles of all investigated waxes decrease by approximately 70° , which indicates a much better wettability compared to their initial properties. Another important effect regarding the sensor fabrication is that the wetting properties do not change significantly over time. Eighteen hours after plasma treatment, an increase in contact angle by a maximum of 15° is observable, but this has no relevant influence on further process steps.

C. Sensor Element—Design and Fabrication

The temperature sensor elements substrate is a custom-designed printed circuit board (PCB). The PCB layout consists of a single conductor with the dimensions of $4 \times 20\text{ mm}$ (width \times length), which is separated by a central hole with a diameter of 4 mm. Both parts of the conductor have a plated through-hole (diameter 1 mm) with a pitch of 15.24 mm, which guarantees an easy pin connection to standard breadboards. The fluidic resistor is made of poly(methyl methacrylate) (PMMA) (topacryl, hesaglas, Switzerland) with a thickness of 1 mm. For cutting and structuring the resistor, a laser-cutting device (Trotec—Speedy100, Germany) was used. Afterward, the resistor was glued to the bottom side of the PCB by a two-component epoxy resin (UHU plus endfest 300, UHU GmbH & Co. KG, Bühl, Germany) [Fig. 4(a)]. In order to fill the wax reservoir, the PCB's surface was coated with one layer of tape (Scotch Magic, 3M, USA) leaving a central hole with a diameter of 6 mm, as illustrated in Fig. 4(b). The same tape was also used to seal the fluidic resistor's outlet. After filling the reservoir with solid wax pieces, the sensor element was put on a hotplate, whose temperature was set 10 K above the respective wax melting point [Fig. 4(c)]. When the wax became liquid, a microscopy slide was used to remove excess material and to create a smooth surface. Afterward, the sensor element was exposed to an oxygen plasma at an operation power of 20 W and an oxygen flow of 20 sccm for 120 s [Fig. 4(d)]. Immediately after plasma surface modification,

TABLE I
THERMAL CHARACTERISTICS OF USED WAXES

Name	Wax	Supplier	Dropping point in °C (datasheet)	Melting point in °C (measured)
Wax 1	Roti-Plast 55	Carl Roth GmbH	54-56	56.7
Wax 2	Tudamelt 64/66	H&R Group	64-66	66.9
Wax 3	Tudamelt MW 8030	H&R Group	72-74	77.1
Wax 4	Deurex H91K	Deurex AG	110-120	112.6
Wax 5	Deurex H92	Deurex AG	130-140	139.2

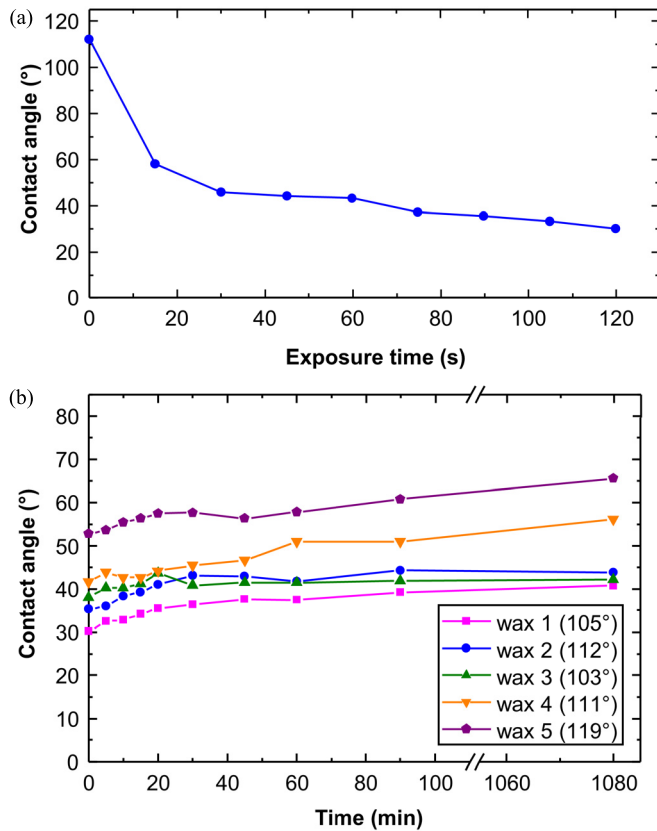


Fig. 3. (a) Contact angle of wax 2 over plasma exposure time. (b) Contact angle of the wax surfaces after surface modification over time (initial contact angle is given in brackets). The values at $t = 0$ s correspond to the contact angles directly after plasma modification.

all coating tapes were removed and the inkjet printing was initiated (Fujifilm Dimatix, Tokyo, Japan—DMP-2800). In three consecutive print runs, silver nanoparticle ink (NanoDimension, Ness Ziona, Israel—SilverNanoParticle Ink, Batch 418) was printed on the wax reservoir's surface with a resolution of 635 dpi [Fig. 4(e)]. As proposed in [23], the stripes conductivity was established by printing another layer of NaCl solution (4 mol/L, 1270 dpi) on top [Fig. 4(f)]. This led to an average resistance of 4Ω between the PCB's electrodes. Finally, a layer of absorbing tissue (PC68, Vipera, Braunschweig, Germany) was attached at the bottom of the sensor element. For experimental investigations, four of these sensor elements were integrated into a single PCB.

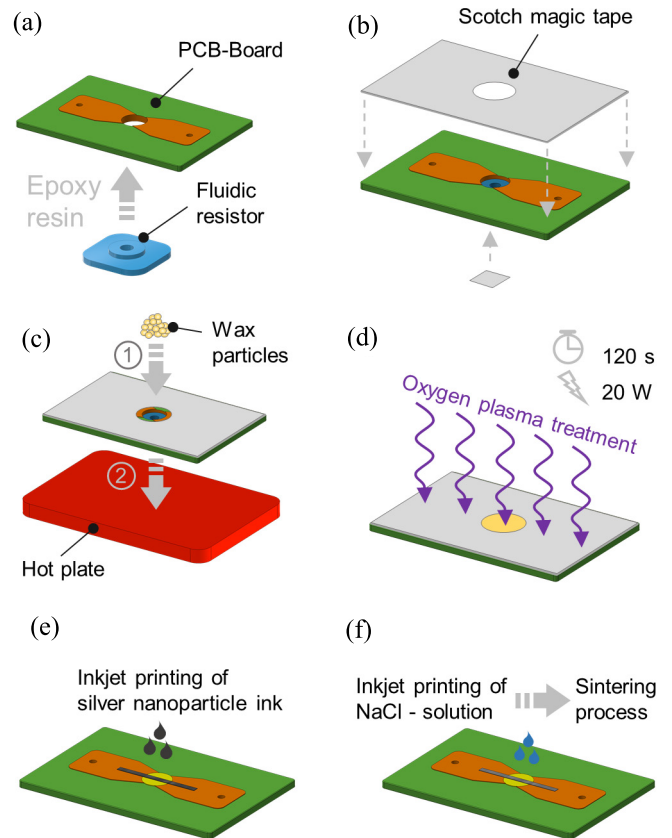


Fig. 4. Major fabrication steps of the sensor element: (a) adding fluidic resistor; (b) covering the sensor surface for wax application; (c) incorporating and melting of wax particles; (d) plasma treatment; (e) inkjet printing of silver nanoparticle ink; and (f) sintering of silver ink by printing an additional layer of NaCl solution.

D. Experimental Setup

The sensor element switching behavior was characterized by the setup shown in Fig. 5. A temperature-controlled measurement chamber (HT 7004, Heraeus/Vötsch, Balingen, Germany) served as a testing environment. The samples were connected to a digital multimeter (HP34970A, Agilent/HP, Santa Clara, CA, USA) by heat-resistant wires. The multimeter was used to monitor the sensors' electrical properties and the reference temperature, which was measured by a PT1000 element. A custom-programmed Python software controlled all components. It enabled the setting of user-defined temperature profiles and visualization and storage of all collected data.

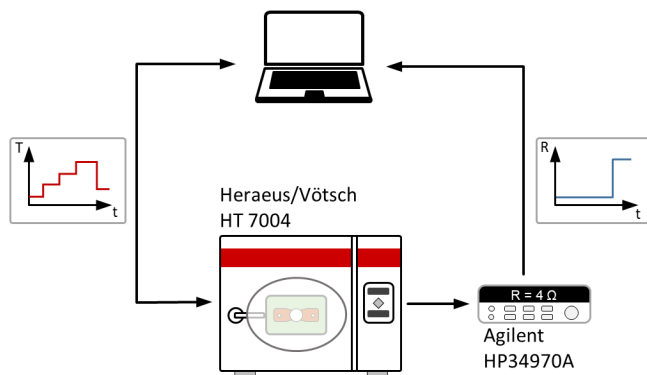


Fig. 5. Schematic representation of the experimental setup for the sensor characterization.

With respect to the thermal capacity of the wax sensors, the temperature was not changed continuously but rather in a ramp function during all experiments. Close to the expected trigger point, the temperature was increased in increments of 1 K. The step width (i.e., time) was adapted to the respective investigation.

IV. RESULTS AND DISCUSSION

A. Temperature Threshold Sensing

The basic response of the fabricated sensor element to a critical temperature exposure is presented in Fig. 6. It shows the sensor resistance over time. The resistance remains in its initial untriggered state as long as the ambient temperature is below the targeted switching temperature. In this state, the resistance is approximately 4Ω . If the temperature gets closer to the critical temperature, the wax surface becomes softer and starts to deform. Small changes in the resistance of the printed silver stripe characterize this region. Exceeding the trigger temperature, the entire wax in the reservoir starts to melt and flows through the fluidic resistor into the absorbing fabric. The descending level of liquid wax causes an irreversible and sudden disruption of the sensor element's electrical connection, which is indicated by a resistance of $10^{12} \Omega$ in all diagrams. In this condition, the sensor is in its triggered state. Table II summarizes the switching temperatures for sensor elements with different wax types and an outlet size of 2 mm. They can detect threshold temperatures in the range from $55 \text{ }^\circ\text{C}$ to $140 \text{ }^\circ\text{C}$ with a high reproducibility. Only wax 4 shows an increased standard deviation, which is caused by its poorer wettability with the silver ink.

B. Temperature- and Time-Dependent Switching

Sensor elements with three different outlet sizes were fabricated to investigate the fluidic resistor influence on the switching characteristics. The manufactured evaluation boards consisted of four sensor elements with the same outlet size and wax type. In total, three circuit boards with 12 sensor elements were measured simultaneously for one wax type. The resulting data are presented in Fig. 7 exemplary for wax 5. As expected, smaller outlet diameters increase the sensor elements' trigger time under critical temperature exposure. In fact, the sensors in

TABLE II
SWITCHING TEMPERATURES OF DIFFERENT WAXES
(OUTLET SIZE OF 2 mm)

Wax	Melting point ($^\circ\text{C}$)	Switching temperature ($^\circ\text{C}$)	Standard deviation (K)
wax 1	56.7	55	0.8
wax 2	66.9	64	0.9
wax 3	77.1	76	1.0
wax 4	112.6	106	6.7
wax 5	139.2	140	1.0

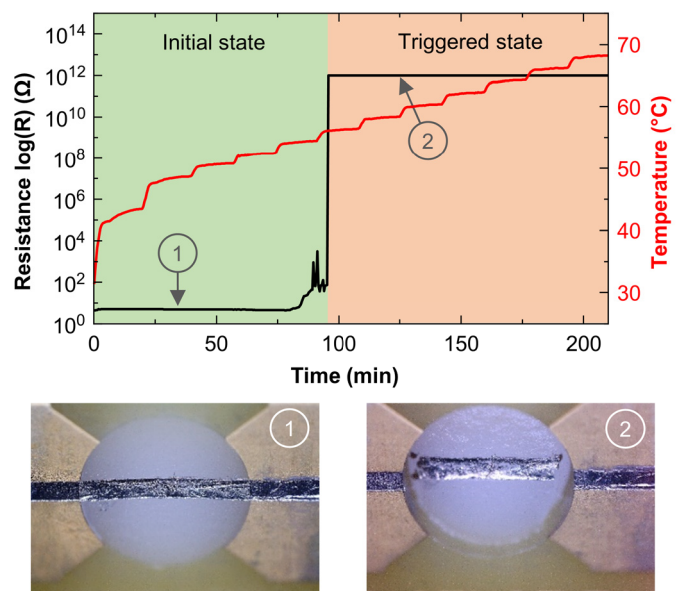


Fig. 6. Representation of the sensor elements' general switching behavior. In its initial state, the sensor shows a low resistance (1). Exceeding a certain threshold temperature, the wax starts to melt and the conductive layer is interrupted. This characterizes the sensor-triggered state (2).

Fig. 7 offer a time delay in the range of 4 min 30 s (2.0 mm) to 12 min 6 s (1.0 mm) after exceeding the trigger temperature. Further data for three waxes with different melting points are provided in Fig. 8. Although the basic relation between outlet diameter and trigger time is similar, each wax has a specific trigger delay. This seems to be affected by the type of wax, especially by its composition.

However, one property is the same for all waxes. The trigger time standard deviation is in the range of 1–2 min for all samples. This is caused by the melting properties of wax in general and leads in relation to the trigger time to a more reliable switching behavior for sensors with smaller outlet diameters.

The sensors' reaction to a short violation of the threshold temperature is depicted in Fig. 9. Exceeding the switching temperature by a maximum of 1 K for 60 s does not lead to a

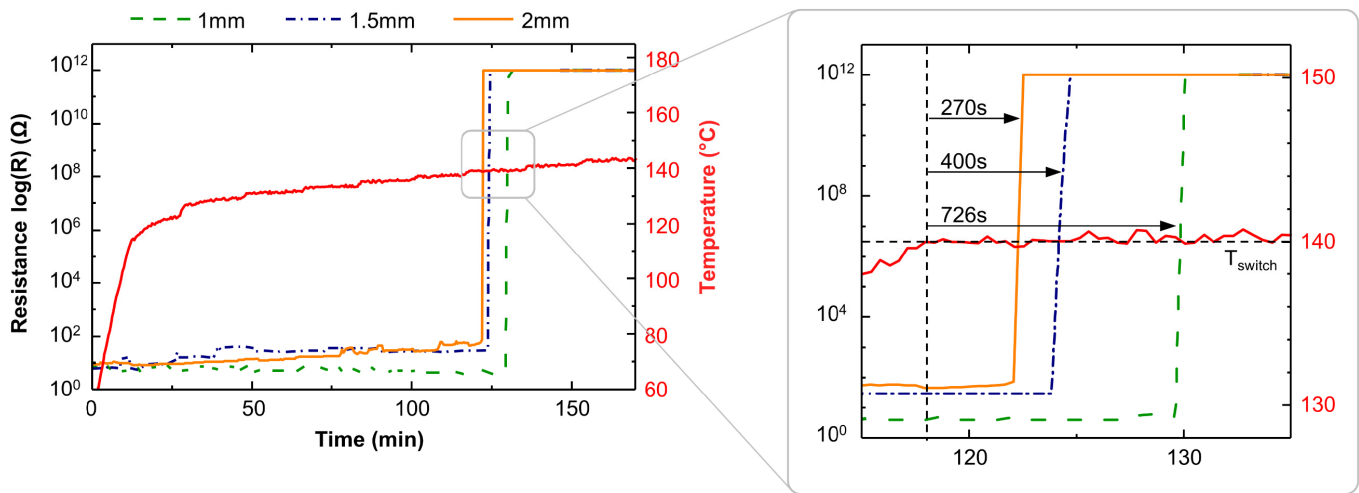


Fig. 7. Switching characteristics of a sensor element with wax 5 and three different outlet sizes. The detailed view of the data clearly shows that an increase in the outlet diameter leads to an earlier trigger event.

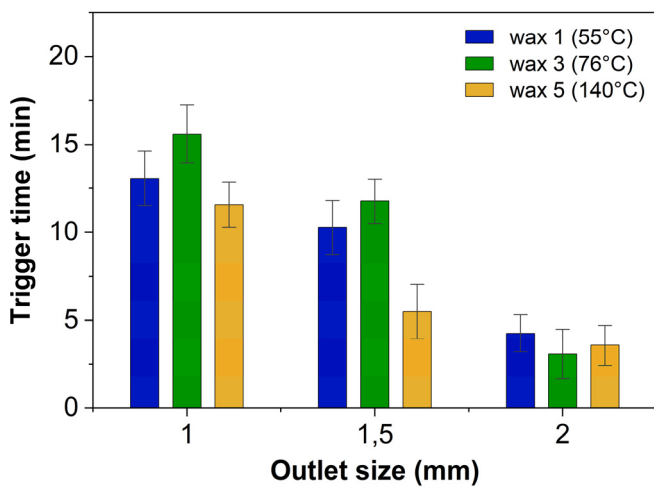


Fig. 8. Summary of the trigger time for sensors with different waxes and outlet sizes.

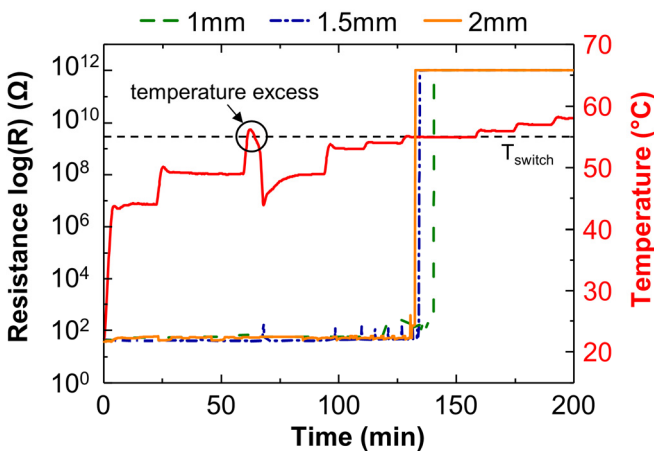


Fig. 9. Sensor behavior after short exceedance of their trigger temperature (wax 1).

premature triggering. However, a closer look at the data reveals that the sensors switched slightly earlier to the triggered state compared to previous experiments.

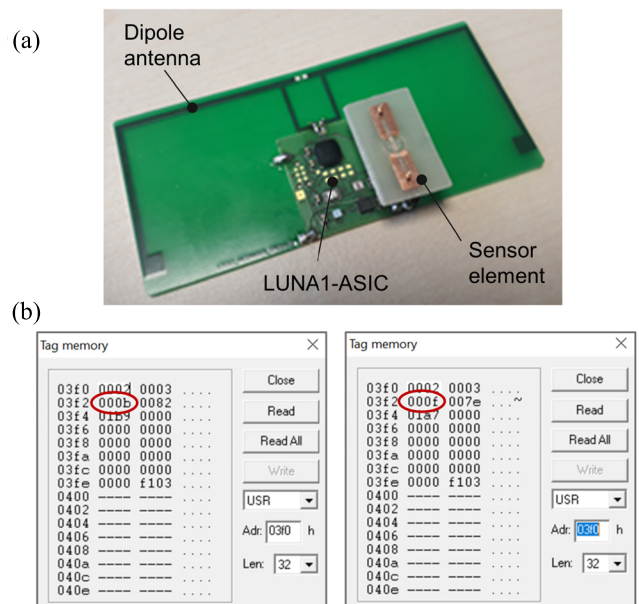


Fig. 10. (a) System setup with LUNA1-ASIC, mounted sensor element, and dipole antenna. (b) Memory readout for untriggered (left) and triggered sensor element (right).

To further investigate this effect, four sensors filled with wax 1 and outlet diameters of 1 and 2 mm were preconditioned 1 K above their switching temperature for 120 s. Afterward, they were tested simultaneously with untreated sensors with the same specifications. The results showed that the trigger time of preconditioned samples was 40% lower than that of untreated sensor elements, regardless of their outlet diameter. This means that short threshold exceedances do not lead to a premature trigger event but cause a kind of memory effect that reduces the trigger time for future temperature threshold violations.

C. System Testing

To demonstrate the sensor elements' capability to work in a passive RFID-tag sensor system, it was attached by plug-in

connectors to a PCB containing the ASIC LUNA1 and a planar dipole antenna [Fig. 10(a)]. Apart from the antenna, the LUNA1 ASIC, and the sensor element, no additional components are required for temperature threshold monitoring. To read the sensor state, the system is brought into the electromagnetic field of an ISO 18000-6 RFID reader. Using the provided field energy, the transponder ASIC constantly queries the status of the sensor and stores the information 0 or 1 in the memory area. Fig. 10(b) shows the memory representation of the transponder ASIC for both cases—the untriggered (left) and triggered sensor states (right). Up to four threshold value, sensors can be queried in the low-order tuple of the marked memory word.

V. CONCLUSION

The transport of sensitive goods via global supply chains makes monitoring of environmental parameters indispensable. Cost-effective and energy-autonomous sensors or sensors without permanent energy supply play a particularly important role. The sensor concept introduced in this article enables easy and reliable detection of critical temperature events. In addition, this sensor element provides the possibility to define the permissible duration of a critical temperature exposure. Upon such an event, the sensor reacts with an irreversible change in resistance that occurs over several decades. This information can be easily detected and transmitted by special RFID circuits with a digital input such as the herein-utilized LUNA1-ASIC.

While the presented results demonstrate the feasibility of the proposed sensor design, there are still some issues that require further attention. In detail, the design of the conducting layer in the transition area between PCB and wax surface should be improved to enhance the reliability of the sensor. The current design of the fluidic resistor is the first approach to test the working principle. At this point, further investigation is needed in terms of material combinations and outlet design to improve the delay characteristics of the sensing element. In order to extend the application range to lower temperatures, the use of other waxes or materials such as oils or greases is conceivable. However, in combination with the good scalability of the sensor design, the developed concept represents a good opportunity for low-cost temperature threshold monitoring with passive ISO 18000-6 conform RFID tags. Possible future areas of application could be in the field of life-cycle monitoring at a product level or smart packaging applications.

REFERENCES

- [1] (2013). *Food Wastage Footprint: Impacts on Natural Resources*. FAO, Rome, Italy, 2013. [Online]. Available: <http://gbv.ebilib.com/patron/FullRecord.aspx?p=3239184>
- [2] R. Badia-Melis, U. Mc Carthy, L. Ruiz-Garcia, J. Garcia-Hierro, and J. I. R. Villalba, "New trends in cold chain monitoring applications—A review," *Food Control*, vol. 86, pp. 170–182, Apr. 2018, doi: [10.1016/j.foodcont.2017.11.022](https://doi.org/10.1016/j.foodcont.2017.11.022).
- [3] C. C. Emenike, N. P. Van Eyk, and A. J. Hoffman, "Improving cold chain logistics through RFID temperature sensing and predictive modelling," in *Proc. IEEE 19th Int. Conf. Intell. Transp. Syst. (ITSC)*, Rio de Janeiro, Brazil, Nov. 2016, pp. 2331–2338, doi: [10.1109/ITSC.2016.7795932](https://doi.org/10.1109/ITSC.2016.7795932).
- [4] N. I. Shchurov et al., "Degradation of lithium-ion batteries in an electric transport complex," *Energies*, vol. 14, no. 23, p. 8072, Dec. 2021, doi: [10.3390/en14238072](https://doi.org/10.3390/en14238072).
- [5] F. Leng, C. M. Tan, and M. Pecht, "Effect of temperature on the aging rate of Li ion battery operating above room temperature," *Sci. Rep.*, vol. 5, no. 1, p. 12967, Aug. 2015, doi: [10.1038/srep12967](https://doi.org/10.1038/srep12967).
- [6] A. A. Zaher, "Smart temperature sensors: History, current practices, and future trends," in *Process Analysis, Design, and Intensification in Microfluidics and Chemical Engineering* (Advances in Chemical and Materials Engineering), J. Davim, H. S. Santana, J. D. L. Silva Jr., and O. P. Taranto, Eds. Pennsylvania, PA, USA: IGI Global, 2019, pp. 223–250.
- [7] S. Wang, J. Tang, and F. Younce, "Temperature measurement," in *Encyclopedia of Agricultural, Food, and Biological Engineering*. New York, NY, USA: Marcel Dekker, 2003, pp. 987–993.
- [8] S. Wang, X. Liu, M. Yang, Y. Zhang, K. Xiang, and R. Tang, "Review of time temperature indicators as quality monitors in food packaging," *Packag. Technol. Sci.*, vol. 28, no. 10, pp. 839–867, Oct. 2015, doi: [10.1002/pts.2148](https://doi.org/10.1002/pts.2148).
- [9] C. E. Sing, J. Kunzelman, and C. Weder, "Time-temperature indicators for high temperature applications," *J. Mater. Chem.*, vol. 19, no. 1, pp. 104–110, 2009, doi: [10.1039/b813644k](https://doi.org/10.1039/b813644k).
- [10] M. Shetty, "Time temperature indicators for monitoring environment parameters during transport and storage of perishables: A review," *Environ. Conservation J.*, vol. 19, no. 3, pp. 101–106, Dec. 2018, doi: [10.36953/ecj.2018.19313](https://doi.org/10.36953/ecj.2018.19313).
- [11] R. Bhattacharyya, C. Floerkemeier, and S. Sarma, "RFID tag antenna based temperature sensing," in *Proc. IEEE Int. Conf. RFID*, Orlando, FL, USA, Apr. 2010, pp. 8–15, doi: [10.1109/RFID.2010.5467239](https://doi.org/10.1109/RFID.2010.5467239).
- [12] F. Vivaldi et al., "A temperature-sensitive RFID tag for the identification of cold chain failures," *Sens. Actuators A, Phys.*, vol. 313, Oct. 2020, Art. no. 112182, doi: [10.1016/j.sna.2020.112182](https://doi.org/10.1016/j.sna.2020.112182).
- [13] A. A. Babar, S. Manzari, L. Sydanheimo, A. Z. Elsherbeni, and L. Ukkonen, "Passive UHF RFID tag for heat sensing applications," *IEEE Trans. Antennas Propag.*, vol. 60, no. 9, pp. 4056–4064, Sep. 2012, doi: [10.1109/TAP.2012.2207045](https://doi.org/10.1109/TAP.2012.2207045).
- [14] T. Athauda, R. Bhattacharyya, N. Karmakar, and S. Sarma, "Electromagnetic characterization of a food safe, organic smart material for customizable temperature threshold sensing in cold chain applications," in *Proc. IEEE Int. Conf. RFID (RFID)*, Phoenix, AZ, USA, Apr. 2019, pp. 1–6, doi: [10.1109/RFID.2019.8719251](https://doi.org/10.1109/RFID.2019.8719251).
- [15] Z. Khan, X. Chen, H. He, A. Mehmood, and J. Virkki, "A bending passive RFID tag as a sensor for high-temperature exposure," *Int. J. Antennas Propag.*, vol. 2021, pp. 1–9, Apr. 2021, doi: [10.1155/2021/5541197](https://doi.org/10.1155/2021/5541197).
- [16] A. Heinig, A. E. Viegas, A. Weder, and M. Czernohorsky. (2023). *RFID Sensor Transponder With Antiferroelectric Embedded Thin Film Capacitors*. [Online]. Available: <https://www.mikrosystemtechnik-kongress.de/proceedings-18a5b24>
- [17] A. Heinig, "Energieautarke RFID-sensorsysteme für die Industrie 4.0: Sachbericht zum abschluss," Fraunhofer Inst. Photon. Microsyst., Dresden, Germany, Project Rep., 2021, doi: [10.2314/KXP:1815527781](https://doi.org/10.2314/KXP:1815527781).
- [18] A. W. Christiansen, "How overdrying wood reduces its bonding to phenol-formaldehyde adhesives: A critical review of the literature. Part I. Physical responses," *Wood Fiber Sci.*, vol. 22, no. 4, pp. 441–459, Oct. 1990. [Online]. Available: <https://wfs.swst.org/index.php/wfs/article/view/2105>
- [19] R. Kurt, A. Krause, H. Militz, and C. Mai, "Hydroxymethylated resorcinol (HMR) priming agent for improved bondability of wax-treated wood," *Holz Als Roh-Und Werkstoff*, vol. 66, no. 5, pp. 333–338, Oct. 2008, doi: [10.1007/s00107-008-0265-1](https://doi.org/10.1007/s00107-008-0265-1).
- [20] U. Kogelschatz, "Dielectric-barrier discharges: Their history, discharge physics, and industrial applications," *Plasma Chem. Plasma Process.*, vol. 23, no. 1, pp. 1–46, 2003, doi: [10.1023/a:1022470901385](https://doi.org/10.1023/a:1022470901385).
- [21] R. Hippler, S. Pfau, M. Schmidt, and K. H. Schoenbach, *Low Temperature Plasma Physics: Fundamental Aspects and Applications*. Weinheim, Germany: Wiley, 2001, p. 530.
- [22] G. Avramidis, G. Scholz, E. Nothnick, H. Militz, W. Viöl, and A. Wolkenhauer, "Improved bondability of wax-treated wood following plasma treatment," *Wood Sci. Technol.*, vol. 45, no. 2, pp. 359–368, May 2011, doi: [10.1007/s00226-010-0327-5](https://doi.org/10.1007/s00226-010-0327-5).
- [23] S. Sauer and W.-J. Fischer, "An irreversible single-use humidity-threshold monitoring sensor principle for wireless passive sensor solutions," *IEEE Sensors J.*, vol. 16, no. 18, pp. 6920–6930, Sep. 2016, doi: [10.1109/JSEN.2016.2590837](https://doi.org/10.1109/JSEN.2016.2590837).



René Körbitz received the Dipl.-Ing. degree in electrical engineering from the Technische Universität Dresden (TUD), Dresden, Germany, in 2011, where he is currently pursuing the Ph.D. degree with the Institute of Semiconductors and Microsystems.

He is also working as a Research Associate with TUD. For several years, he had been working in the field of microfluidics and microsystems before he has been dealing with shape memory alloys for medical applications.



Wolf-Joachim Fischer (Life Senior Member, IEEE) was born in Dresden, Germany, in 1950. He received the Diploma and Ph.D. degrees in electrical engineering from the University of Technology Dresden, Dresden, in 1973 and 1976, respectively.

From 1973 to 1991, he was with ZMD Inc., Dresden, where he was engaged in the design of integrated circuits. In 1991, he joined the Fraunhofer Institute for Microelectronic Circuits and Systems, Duisburg, Germany, where he led the Department of IC Design. Since 1994, he has been a Professor of Microsystems Technology with the Faculty of Electrical and Computer Engineering, Dresden. Dr. Fischer has authored three books and more than 100 articles, and holds several patents. His main research interests include intelligent microsystems and wireless sensor systems.



Andreas Heinig was born in Altenburg, Germany, in 1968. He received the degree in electrical engineering from the Technical University of Dresden, Dresden, Germany, in 1995, and the Ph.D. degree in microsystems technology from Technische Universität Dresden, Dresden, with the topic "use of cryptographic algorithms in microsystems technology and microelectronics considering clocked and self-synchronizing circuit technology," in 2000.

He qualified as an Electronic Technician specializing in construction and functional groups. Since 1995, he has been working in various positions with the Fraunhofer Institute for Microelectronic Circuits and Systems, Duisburg, Germany, and later with the Fraunhofer Institute for Photonic Microsystems, Dresden. He deals with the system and circuit design of microelectronic systems as well as with antenna design.